Research on integrated motion and vibration control methods for heated nozzles in space additive manufacturing equipment

Yuchen Yang[1], Yubin Fang[2]
School of Mechanical Engineering, Jiangsu University of Technology, Changzhou, China
[2]Corresponding author
E-mail: [1]*1589060151@qq.com*, [2]*fangyubin91@163.com*

Received 29 July 2025; accepted 12 February 2026; published online 3 March 2026
DOI https://doi.org/10.21595/jve.2026.25227

Abstract. In microgravity and disturbance-rich orbital environments, the thermal nozzle of Delta-type space-based fused deposition modeling (FDM) systems is prone to trajectory deviations and vibration-induced defects, which can severely degrade the surface quality and mechanical integrity of printed parts. To address this problem, an integrated motion-vibration control strategy is proposed. The motion loop employs a classical PID controller for accurate trajectory tracking, whereas the vibration loop adopts a Filtered-X Least Mean Square (FXLMS) algorithm with a nonlinear variable step-size scheme jointly modulated by exponential decay and sinusoidal functions. The proposed step-size mechanism improves convergence behavior and robustness under time-varying disturbances by enabling fast initial adaptation while maintaining stable steady-state performance. A high-fidelity ADAMS-Simulink co-simulation platform is developed for comparative evaluation. The results show that the proposed strategy reduces micro-vibration amplitudes, improves tracking accuracy, and provides stronger robustness than fixed-step adaptive approaches, thereby offering an effective solution for high-precision space-based additive manufacturing.

Keywords: space-based additive manufacturing, delta-type FDM, FXLMS algorithm, adaptive vibration suppression, thermal nozzle.

1. Introduction

In recent years, space stations and orbital platforms have entered extended operational phases. Major spacefaring nations have increasingly focused on the construction, maintenance, and autonomous operation of these platforms as core components of long-term aerospace strategy. The United States, China, and Russia have accelerated the deployment of orbital facilities to enable long-duration missions while reducing dependence on ground-based logistics. Against this backdrop, space-based Additive Manufacturing (AM) has emerged as a critical technology for on-orbit repair, rapid component replacement, and structural adaptation, offering significant improvements in mission resilience and logistical efficiency [1], [2]. However, extensive research has shown that inherent microgravity-induced micro-vibrations can significantly degrade manufacturing quality and dimensional accuracy, particularly in FDM systems [3]. Moreover, orbital micro-vibrations may couple with lightweight mechanisms, leading to layer misalignment, geometric distortion, and reduced mechanical performance [4], [5]. Therefore, effective suppression of nozzle vibration has become a key prerequisite for ensuring the reliability of AM.

Among existing AM technologies, FDM is considered highly suitable for microgravity environments due to its compact structure, high reliability, broad material compatibility, and low energy consumption. Meanwhile, Delta-type parallel mechanisms – characterized by lightweight truss structures, high acceleration capability, and excellent motion agility – exhibit strong potential for performing precise and efficient fabrication tasks in space [6]-[8]. However, the inherent structural flexibility and strong kinematic coupling of Delta mechanisms make them susceptible to vibration amplification during high-speed motion, rapid acceleration/deceleration, and external

disturbances, which further exacerbate trajectory deviations of the thermal nozzle [9], [10].

To mitigate performance degradation caused by vibration, researchers have explored structural damping, compliant mechanisms, and passive isolation techniques. Nonetheless, passive approaches are fundamentally constrained by spacecraft mass, volume, and layout limitations, and exhibit limited effectiveness against broadband, multi-source disturbances. As a result, active vibration control has become an important research direction for space manufacturing systems. Adaptive filtering algorithms such as Least Mean Square (LMS), Normalized least mean square (NLMS), and FXLMS have been extensively applied in space micro-vibration suppression due to their robustness to model uncertainties and broadband disturbances [11]-[13]. Recent studies indicate that disturbances in orbital platforms typically exhibit multi-frequency, broadband, and slowly time-varying characteristics, which pose significant challenges for FXLMS algorithm, often resulting in slow convergence or reduced steady-state accuracy under dynamic conditions [14], [15].

Meanwhile, Delta mechanisms are highly sensitive to actuator noise, structural flexibility, and dynamic coupling during high-speed operations. Prior studies have demonstrated that even minor actuator disturbances can propagate rapidly along the parallel kinematic chains and become amplified [16]. Furthermore, separately addressing trajectory tracking and vibration suppression often fails to meet the simultaneous accuracy and stability requirements under complex operational environments [17]. Taken together, these findings underscore the necessity of a unified control framework capable of simultaneously addressing motion control and vibration suppression in space-based Delta-FDM systems subject to multi-frequency broadband disturbances.

Motivated by these challenges, this study proposes an integrated motion-vibration control strategy for the thermal nozzle of a space-based Delta-type FDM system. The method incorporates a Proportional-Integral-Derivative (PID) motion controller and an enhanced FXLMS algorithm into a unified feedback structure. To address the classical trade-off between convergence speed and steady-state accuracy in FXLMS under dynamic space disturbances, we introduce a nonlinear variable step-size mechanism combining exponential decay with sinusoidal modulation. This design significantly improves convergence stability, transient performance, and robustness against multi-frequency broadband disturbances [18], [19].

A high-fidelity co-simulation platform integrating ADAMS and Simulink was constructed to model the three-degree-of-freedom dynamics of the thermal nozzle and validate the proposed control strategy. Simulation results demonstrate that the Exponential Sinusoidal Filtered-X Least Mean Square (ES-FXLMS) based integrated controller achieves substantial improvements in trajectory tracking accuracy, vibration amplitude suppression, and dynamic adaptability. Compared with traditional PID, NLMS, and standard FXLMS algorithms, the proposed method exhibits superior convergence behavior, disturbance rejection capability, and overall system stability, offering an efficient and robust real-time control solution for space-based additive manufacturing systems [20]-[22].

To facilitate a clearer and more systematic comparison with recent studies on space-based vibration suppression, Table 1 summarizes the representative control strategies, disturbance frequency characteristics, attenuation performance, and experimental or simulation conditions reported in the literature. As can be observed, most existing works primarily focus on single-frequency or narrow-band disturbances, while limited attention has been devoted to the multi-frequency and broadband excitations that are commonly encountered in space-based environments.

Motivated by these observations, this study develops an integrated motion-vibration control strategy for the thermal nozzle of a space-based Delta-type FDM system. The proposed framework combines classical PID trajectory control with an enhanced ES-FXLMS adaptive vibration suppression algorithm, aiming to achieve effective vibration attenuation and accurate motion tracking under multi-frequency, broadband, and time-varying disturbance conditions.

Table 1. Comparison between our method and some published methods

Reference	Control strategy	Disturbance frequency bands	Attenuation (dB)	Experimental scenario
[11]	LMS / FXLMS	Single-frequency	0-40 dB	Space instruments (Earth-based test)
[12]	VSS-FXLMS	Broadband	0-50 dB	Flexible structures (Lab-based)
[13]	LMS variants	Dual-frequency	0-35 dB	Robotic arm (Laboratory)
[16]	Dynamic modeling	N/A	N/A	Delta robot (Model-based)
[4]	Disturbance modeling	Micro-vibration	0-60 dB	Space AM (Simulation)
This work	PID+ES-FXLMS	Dual-frequency + Broadband	> 70 dB	Space FDM (Delta) + ADAMS-Simulink Co-simulation

2. Vibration characteristic analysis of the thermal nozzle in delta-type additive manufacturing equipment

2.1. Basic working principle of the thermal nozzle

The working principle of FDM additive manufacturing is based on heating a thermoplastic material to its molten state and then precisely extruding it through a thermal nozzle to construct three-dimensional objects layer by layer. The process begins with the filament being fed into the heated nozzle by a feeding mechanism, where it is melted and subsequently extruded along a predefined path. Each layer of molten material solidifies upon cooling and is deposited sequentially to form the complete object [23].

FDM systems are widely used in prototyping and functional part fabrication due to their simple structure, user-friendly operation, and broad material compatibility. These characteristics make FDM particularly suitable for environments with limited space, such as homes and educational institutions. Owing to their ease of use and low cost, PID control is widely used in FDM devices due to its simplicity and reliability. As illustrated in Fig. 1.

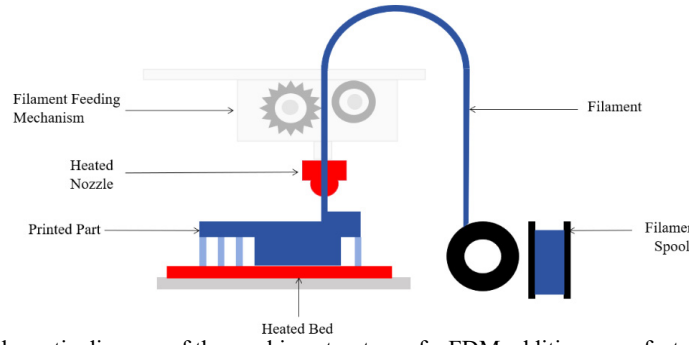

Fig. 1. Schematic diagram of the working structure of a FDM additive manufacturing system

2.2. Dynamic modeling of delta-type additive manufacturing equipment

Dynamic analysis is essential for both performance evaluation and motion control of parallel robotic systems, as it characterizes the relationship between joint actuation and system motion states. Forward dynamics analysis is primarily used for system simulation and performance validation, whereas inverse dynamics provides the theoretical basis for controller design. An accurate dynamic model not only enables deeper insight into the robot's dynamic behavior but also supports the development of high-speed, high-precision trajectory planning and control algorithms. The dynamic configuration of the Delta-type mechanism considered in this study is illustrated in Fig. 2.

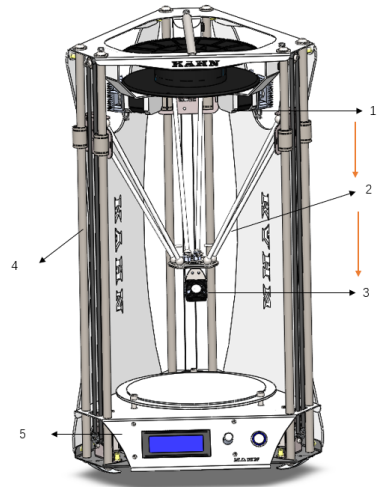

Fig. 2. Schematic diagram of the delta-type additive manufacturing structure:
1 – drive motor; 2 – linkage; 3 – thermal nozzle actuator; 4 – lead screw; 5 – base

To characterize the high-frequency micro-vibration behavior of the thermal nozzle during space-based FDM printing, the nozzle and its supporting end-effector platform are modeled as an equivalent lumped mass m, as shown in Fig. 3. A local Cartesian coordinate system is established at the center of mass to describe translational motions along the horizontal x-axis, y-axis and the vertical z-axis. For vibration suppression analysis, the system is further simplified as a three-degree-of-freedom lumped-parameter model.

The mechanical compliance of the Delta mechanism, including the flexibility of the three driving limbs and the upper platform, is represented by three independent linear elastic and damping elements. The equivalent stiffness and damping coefficients along each axis are denoted as k_x, k_y, k_z and c_x, c_y, c_z, respectively. During printing, the nozzle is subject to external excitations – such as structural vibrations, actuator-induced disturbances, and base micro-vibrations – which are lumped as generalized forces $F_x(t)$, $F_y(t)$, and $F_z(t)$.

Under the small-amplitude vibration assumption, the dynamics of the nozzle can be linearized and formulated as a three-degree-of-freedom lumped-parameter model:

$$\begin{aligned} m_x\ddot{x} + c_x\dot{x} + k_x &= F_x(t), \\ m_y\ddot{y} + c_y\dot{y} + k_y &= F_y(t), \\ m_z\ddot{z} + c_z\dot{z} + k_z &= F_z(t). \end{aligned} \tag{1}$$

These equations can be written in matrix form as:

$$M\ddot{q} + C\dot{q} + Kq = F(t), \tag{2}$$

where $q = [x, y, z]^T$ denotes the nozzle displacement vector, M, C, K are the equivalent mass, damping and stiffness matrices, and $F(t) = [F_x(t), F_y(t), F_z(t)]^T$ represents the generalized disturbance forces.

This 3-DOF dynamic model provides the physical foundation for the subsequent ES-FXLMS vibration suppression algorithm and establishes a clear link between the Delta mechanism and its vibration-response characteristics.

Although the mass m can be obtained numerically, the computation is complex and inefficient. Therefore, this study derives the dynamic model of the Delta mechanism using the principle of virtual work.

The principle of virtual work applied to n rigid bodies can be expressed as follows:

$$\sum_{i=1}^{N}[(m_i\ddot{x}_i - F_i)\cdot\delta x_i + (I_i\dot{\omega}_i + \omega_i \times I_i\omega_i - T_i)\cdot\delta\phi_i] = 0, \tag{3}$$

where, m_i and I_i denote the mass and inertia matrix of the i rigid body, respectively; $\ddot{x}_i$ represents the linear acceleration of its center of mass; ω_i and $\dot{\omega}_i$ are the angular velocity and angular acceleration; F_i and T_i denote the external force and torque applied to the rigid body; δx_i and $\delta\phi_i$ are the corresponding virtual displacements.

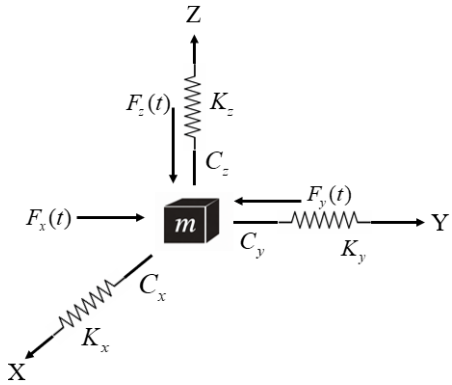

Fig. 3. Simplified three-degree-of-freedom lumped-parameter dynamic model of the thermal nozzle, including equivalent mass, stiffness, damping, and external disturbance forces

For virtual displacements such as δx_i and $\delta\phi_i$, they can be transformed into functions of the virtual joint displacements through the Jacobian matrix. Thus, we obtain:

$$\sum_{i=1}^{N}\left[\delta q^T J_{v,i}^T(m_i\ddot{x}_i - F_i) + \delta q^T J_{\omega,i}^T(I_i\dot{\omega}_i + \omega_i \times I_i\omega_i - T_i)\right] = 0. \tag{4}$$

Therefore, since Eq. (4) holds for any virtual displacement δq, it follows that:

$$\sum_{i=1}^{N}\left[J_{v,i}^T(m_i\ddot{x}_i - F_i) + J_{\omega,i}^T(I_i\dot{\omega}_i + \omega_i \times I_i\omega_i - T_i)\right] = 0. \tag{5}$$

The applied forces include the joint driving torque τ as well as other external forces $F_{i,ext}$ and external torques $T_{i,ext}$. Thus, we have:

$$F_i = \tau + F_{i,ext} + T_{i.ext}. \tag{6}$$

Thus, the dynamic equation can be expressed as follows:

$$\tau = J_\tau^{-1}\left[\sum_{i=1}^{N}\left(J_{v,i}^T m_i\ddot{x}_i + J_{\omega,i}^T(I_i\dot{\omega}_i + \omega_i \times I_i\omega_i)\right) - \sum_{i=1}^{N}\left(J_{v,i}^T F_{i,\text{ext}} + J_{\omega,i}^T T_{i,\text{ext}}\right)\right]. \tag{7}$$

Given that the primary objective of spaceborne FDM equipment is to suppress micro-vibrations induced by the coupling between motion and external disturbances, the fundamental cause of these vibrations lies in the intrinsic dynamic characteristics of the structure, which remain unchanged in a microgravity environment. According to existing studies on the dynamics of space structures [24], the principle of virtual work is a commonly used and effective

approach for analyzing micro-vibration problems in large flexible spacecraft and their appendages. Therefore, the dynamic model established in this work provides a reasonable and reliable basis for investigating the motion and vibration control of space-based FDM systems during on-orbit operation.

In this study, the full multibody dynamics of the Delta mechanism were first derived using the principle of virtual work. This complete model reveals the sources of inertia, coupling, and external disturbances.

However, for the purpose of vibration suppression, the nozzle operates in a small-amplitude micro-vibration region. Therefore, the full nonlinear dynamics are linearized around the operating point and reduced to an equivalent 3-DOF translational mass-spring-damper model:

$$M\ddot{q} + C\dot{q} + Kq = F(t). \tag{8}$$

This linearized model is used throughout the controller design and stability analysis. Within the small-displacement range, the matrices M, C, and Kremain constant, and the system behaves as a lightly damped second-order system with all poles in the left-half complex plane. The PID controller further shifts the closed-loop poles leftward, ensuring zero steady-state error and improved damping. Although nonlinear effects (Coriolis, centrifugal, geometric nonlinearities) are neglected here, they will be evaluated through future Hardware-in-the-loop (HIL) experiments to confirm the applicability of the linear model.

Although the three actuated limbs of the Delta mechanism are driven independently, the parallel kinematic structure inherently introduces inter-axis coupling. Such coupling may potentially affect the end-effector trajectory accuracy, especially under high-speed and large-amplitude motion. To quantitatively assess the influence of coupling terms within the workspace considered in this study, a sensitivity-based analysis was carried out around a representative operating point near the center of the printing workspace.

Small unit perturbations were applied independently to each joint variable q_j, and the resulting changes in the Cartesian nozzle position x_i were recorded. On this basis, normalized sensitivity coefficients were defined as:

$$S_{ij} = \frac{|\Delta x_i/\Delta q_j|}{|\Delta x_i/\Delta q_i|}, \tag{9}$$

where S_{ii} represents the primary sensitivity of axis i to its own joint motion, and S_{ij} $(i \neq j)$ reflects the cross-coupling effect from joint j to axis i. A value of S_{ij} close to zero indicates weak coupling, whereas a value comparable to S_{ii} would imply strong coupling. The computed normalized sensitivity matrix for the analyzed operating region is summarized in Table 2.

Table 2. Normalized joint–axis sensitivity coefficients of the Delta mechanism

Axis/Joint	q_1	q_2	q_3
x	1.00	0.03	0.04
y	0.04	1.00	0.05
z	0.02	0.03	1.00

The results indicate that all off-diagonal sensitivity coefficients S_{ij} $(i \neq j)$ remain below 0.05, less than 5 % of the corresponding primary sensitivities. This is consistent with the modal sensitivity analysis and dynamic simulations performed, where the off-diagonal elements of both the Jacobian matrix and the inertia matrix were found to be less than 5 % of the corresponding diagonal elements. These findings quantitatively confirm that, within the motion ranges considered in this work, the inter-axis coupling is weak.

Because the coupling terms contribute only a small fraction to the overall trajectory deviation, their effect on tracking accuracy can be regarded as second-order. Under the present operating

conditions, this influence is therefore negligible. Therefore, independent PID control is adopted for each axis in this study. This not only simplifies the controller structure and parameter tuning but also improves real-time implementation efficiency without sacrificing trajectory accuracy in the tested workspace.

Nevertheless, it should be emphasized that the proposed framework is not limited to independent control. For future applications involving larger workspaces, higher speeds, or heavier loads, where coupling may become more pronounced – the current scheme can be extended to a multivariable coordinated control structure, for example by incorporating model-based decoupling or adaptive multivariable compensation to further enhance global trajectory accuracy and dynamic consistency.

3. Integrated motion and vibration control design for the thermal nozzle in delta-type additive manufacturing

3.1. Overall architecture design

This paper proposes an integrated control method that combines PID-based motion control with FXLMS-based adaptive vibration suppression, tailored to the motion characteristics and vibration mitigation requirements of the thermal nozzle in Delta-type additive manufacturing systems. The overall system architecture consists of a motion control loop and a vibration suppression loop, which are responsible for precise trajectory tracking and real-time vibration attenuation, respectively. The effectiveness of the proposed control strategy is validated through co-simulation with an Adams model. As illustrated in Fig. 4.

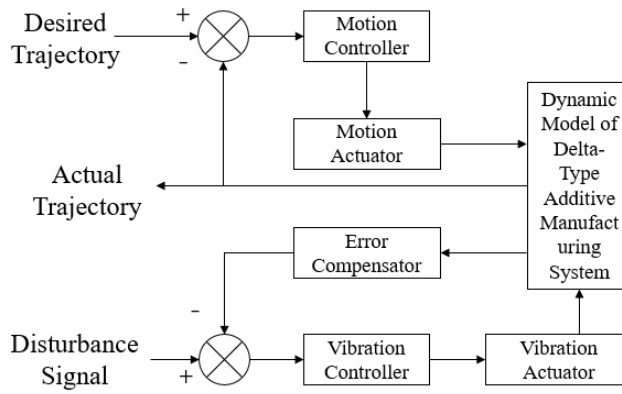

Fig. 4. Block diagram of the integrated motion and vibration control system for the thermal nozzle in delta-type additive manufacturing equipment

3.2. PID motion control

To achieve precise trajectory tracking of the thermal nozzle in three-dimensional space for space-based additive manufacturing equipment, this study adopts a closed-loop feedback strategy based on a PID controller in the motion control loop. As shown in Fig. 5, the PID controller offers a simple structure, strong real-time performance, and ease of tuning, making it effective in improving both system response speed and steady-state accuracy. These advantages make it well-suited to the high-precision motion control requirements of this work.

Based on the dynamic characteristics of the Delta mechanism, the motion of the thermal nozzle can be approximated by the following multi-degree-of-freedom rigid-body dynamic equation:

$$M\ddot{\mathbf{q}}(n) + C\dot{\mathbf{q}}(n) + K\mathbf{q}(n) = -MIw_e(n) + Bu(n), \tag{10}$$

where $\mathbf{q}(n)$ denotes the displacement vector, and $u(n)$ represents the control input. The matrices M, C, and K correspond to the equivalent mass, damping, and stiffness of the system, while B is the input distribution matrix. This equation provides the fundamental dynamic framework required for the PID-based motion control design. The simplified 3-DOF vibration model introduced in Section 2.2 is obtained by linearizing this general form under small-amplitude vibration assumptions.

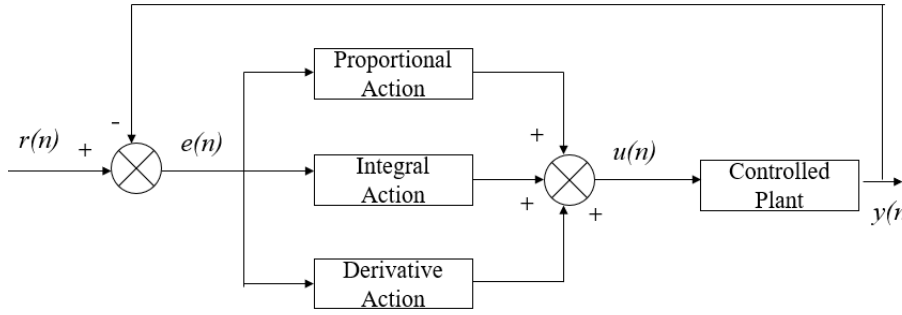

Fig. 5. Schematic diagram of the PID control system

In this system, independent PID control loops are designed for the x, y, and z directions to accommodate the three degrees of freedom of the Delta mechanism's spatial motion. This ensures that the motion trajectories along each axis can independently and synchronously follow the desired reference paths.

3.3. Vibration suppression strategy

Building upon the completed motion control of the thermal nozzle, this study further addresses the vibration issues induced during high-speed operations, which arise from structural flexibility and external micro-disturbances. Although the PID controller can improve the positioning accuracy to some extent, it is fundamentally designed for static error correction and thus lacks the capability to effectively suppress dynamic vibrations that compromise system stability and trajectory accuracy. This limitation is particularly significant in the application environment of Delta-type additive manufacturing systems, where the thermal nozzle structure is lightweight and exhibits limited stiffness. As a result, high-speed motion tends to excite small but persistent vibrations that can severely degrade printing quality.

Therefore, based on the PID motion control framework, this study introduces an adaptive vibration suppression controller using the FXLMS algorithm. By continuously monitoring the vibration error signals during motion, the FXLMS controller dynamically adjusts the compensation signal in real time to actively suppress vibrations at the thermal nozzle tip. This enhances both the stability and accuracy of trajectory tracking.

The motion control and vibration suppression modules are implemented in parallel within the system architecture. While the motion control module is responsible for tracking the desired trajectory, the vibration control module targets the suppression of dynamic micro-vibrations. These two modules work in a complementary manner to form a unified motion and vibration integrated control strategy.

FXLMS is a widely used adaptive filtering algorithm in applications such as active noise and vibration control, system identification, and signal processing. Compared with the FXLMS algorithm, FXLMS explicitly accounts for the dynamics between the actuator and the error sensor by filtering the reference signal through an estimate of the secondary path, which makes it particularly suitable for disturbance rejection in noisy environments.

In the proposed control framework, the adaptive filter coefficients are updated to minimize the measured vibration error, while the filtered reference signal effectively compensates for the

influence of external disturbances and system dynamics on the adaptation process. This filtering mechanism significantly improves the robustness and convergence behavior of the adaptive algorithm when operating under broadband and time-varying disturbance conditions.

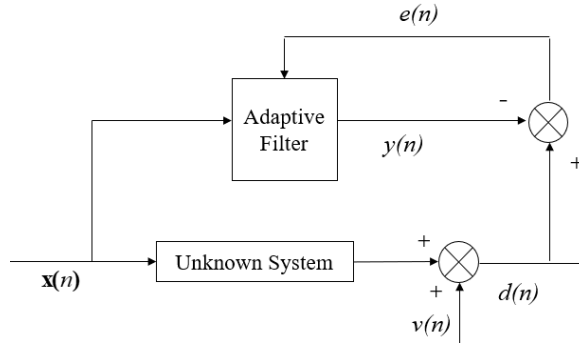

Fig. 6. Schematic diagram of the adaptive filtering principle

A typical adaptive filtering structure is shown in Fig. 6. The notations are defined as follows.

Where $\mathbf{x}(n)$ represents the input signal at time n, $y(n)$ represents the output signal at time n, $d(n)$ represents the desired signal at time n, $e(n)$ represents the error signal, $v(n)$ represents the primary input disturbance signal. After receiving input signal $x(n)$, the output signal $y(n)$ after adaptive filtering is compared with the desired signal $d(n)$, to obtain the error signal $e(n)$, Furthermore, the error signal $e(n)$ is then used to automatically adjust the filter parameters $\mathbf{W}(n)$, In this way, the adaptive filter is gradually adjusted toward convergence, allowing the output $y(n+1)$ at the next time step to more closely approximate the desired signal.

From the principal diagram of the adaptive filter, it is clear that the system's output error is given by:

$$e(n) = d(n) - y(n). \tag{11}$$

The output signal can be expressed as:

$$y(n) = \mathbf{W}(n)^T \mathbf{X}(n). \tag{12}$$

The weight coefficients of the N-th order adaptive filter at time n can be expressed as:

$$\mathbf{W}(n+1) = \mathbf{W}(n) + \mu e(n)\mathbf{X}(n), \tag{13}$$

where μ denotes the step size of the algorithm, and the convergence condition for the LMS algorithm is given by $1 < \mu < \frac{1}{\lambda_{\max}}$, with $\lambda_{\max}$ representing the maximum eigenvalue of the input signal's autocorrelation matrix.

(1) VSSLMS-1 algorithm.

The NLMS algorithm is currently one of the most widely used Variable step-size LMS (VSS-LMS) algorithms [25], [26]. Its step-size update formula is given by:

$$\mu(n) = \frac{\mu}{\mathbf{x}^T(n)\mathbf{x}(n)} = \frac{\mu}{\sum_{i=0}^{L-1} x^2(n-i)}. \tag{14}$$

In the NLMS algorithm, the normalized step size μ must satisfy $0 < \mu < 2$, although smaller values are generally preferred in practical applications to ensure stable adaptation. The algorithm exhibits robustness to variations in the energy of the reference signal $\mathbf{x}(n)$. To enhance numerical stability, particularly to prevent sudden step-size amplification when the reference signal

amplitude approaches zero, which may otherwise destabilize or even cause divergence of the algorithm, a small positive constant ε, much smaller than the reference signal power, is conventionally added to the denominator:

$$\mu(n) = \frac{\mu}{\varepsilon + \mathbf{x}^T(n)\mathbf{x}(n)} = \frac{\mu}{\varepsilon + \sum_{i=0}^{L-1} x^2(n-i)}. \tag{15}$$

(2) VSSLMS-2 algorithm.

A VSS-LMS algorithm based on a nonlinear error function was proposed by F. Wang [27], and its step-size update rule is given by Eqs. (15-16):

$$\mu(n) = \mu(1 - \exp(-\upsilon||\mathbf{x}(n)e(n)||^2))_{\max}, \tag{16}$$

$$\mu(n) = \begin{cases} \mu_{\max}, & \mu'(n) > \mu_{\max}, \\ \mu_{\min}, & \mu'(n) < \mu_{\min}, \\ \mu'(n), & \text{otherwise.} \end{cases} \tag{17}$$

The performance of this algorithm is largely influenced by the value of the damping factor υ. The damping factor determines the duration for which the algorithm operates with a relatively large step size. A larger υ value results in a longer duration of large step-size operation. As υ approaches infinity, the algorithm degenerates into a fixed step-size LMS algorithm.

The computational complexity of an algorithm plays a critical role in its practical applicability, as it directly determines computational efficiency and real-time feasibility. In this section, we compare the computational complexity of several existing VSSLMS algorithms with that of the improved VSSLMS algorithm proposed in this study. The comparison focuses on key indicators such as the number of parameters that must be tuned before execution and the computational load required for step-size updates during each iteration.

In practice, many VSSLMS algorithms require upper and lower bounds on the step size to ensure stable operation. In response to this, we propose an improved variable step-size algorithm (ES-FXLMS), which is formulated as follows:

$$\mu(n) = a * \exp(-b|e(n)|) * \frac{\sin(e(n)) + 1}{2}, \tag{18}$$

where $a \in [0.7, 0.75]$ and $b \in [1, 1.5]$.

Where $e(n)$ represents the vibration control error signal. The parameter a specifies the upper bound of the step size, while b determines the sensitivity of the step-size attenuation with respect to the error magnitude. The exponential term $\exp(-b|e(n)|)$ decreases monotonically as the error grows, ensuring that the adaptation becomes more conservative under large disturbances and preventing unstable gain escalation.

The sinusoidal component $\frac{\sin(e(n))+1}{2}$ provides a smooth, phase-dependent modulation of the step size. This term has been widely used in practical adaptive filtering to avoid abrupt variations in the update gain and to enhance robustness under oscillatory disturbances. Together, these two components form an empirically stable step-size function that provides fast initial convergence when the error is small while maintaining numerical stability during periods of larger or rapidly changing disturbances.

This formulation effectively balances convergence speed and stability, making it well-suited for the time-varying and multi-frequency disturbance environment encountered in space-based FDM systems.

4. Co-simulation study and validation

4.1. Simulation system

To investigate and validate the vibration suppression performance of the thermal nozzle in Delta-type additive manufacturing equipment, a three-degree-of-freedom active vibration control simulation model was established using the dynamic modeling capabilities of ADAMS.

The model consists of two main subsystems: an excitation module and a suppression module. The excitation module simulates micro-vibrations caused by external disturbances, with its output serving as the input to the suppression module. The suppression module, driven by the control algorithm, generates real-time compensation forces to attenuate vibrations effectively.

This model enables simulation of micro-vibrations along the x, y, and z axes. By integrating ADAMS with Simulink via a co-simulation platform and implementing an adaptive filtering-based control algorithm, the effectiveness of the ES-FXLMS Algorithm for vibration suppression was validated in co-simulation. The simulation results suggest a significant reduction in vibration amplitude and improved system stability, as illustrated in Fig. 7.

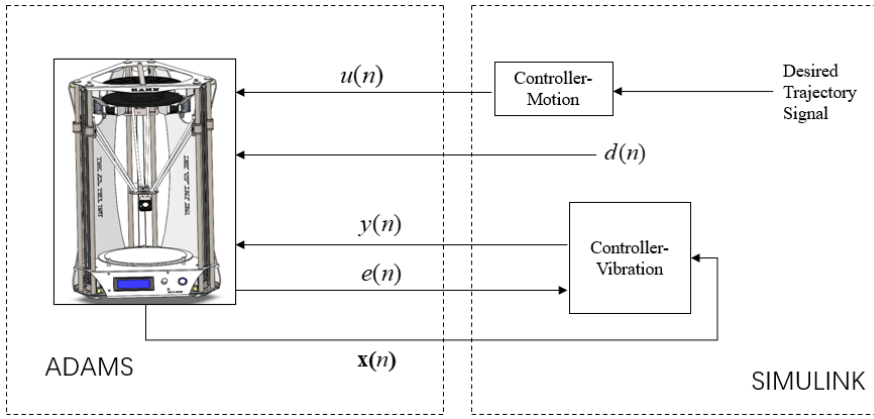

Fig. 7. Co-simulation structure of ADAMS and Simulink

During co-simulation, a single-frequency sinusoidal excitation is introduced in Simulink to mimic realistic disturbances. This signal also serves as the reference input for the control algorithm, facilitating synchronization between excitation and compensation. The PID controller regulates the driving force to minimize trajectory tracking errors.

Meanwhile, ADAMS monitors the displacement at the center of the suppression module's upper surface, which reflects the system's vibrational response. This displacement is fed back to Simulink as an error signal, allowing the adaptive controller to compute a real-time compensation force. The calculated force is applied to the piezoelectric actuator, forming a closed-loop system for active vibration suppression.

The co-simulation environment is built in MATLAB/Simulink. The mechanical model is exported from ADAMS as a script and loaded in MATLAB using the admasses command. Within Simulink, the generated Adams sub-block is inserted into the control framework, as shown in Fig. 8.

To support flexible signal generation and online parameter tuning, a user-defined S-Function module is employed. This module enables custom signal input (e.g., step, sweep) and enhances the scalability of the control system by supporting real-time adjustments. Overall, the co-simulation framework facilitates accurate evaluation of the proposed control algorithm under realistic dynamic conditions.

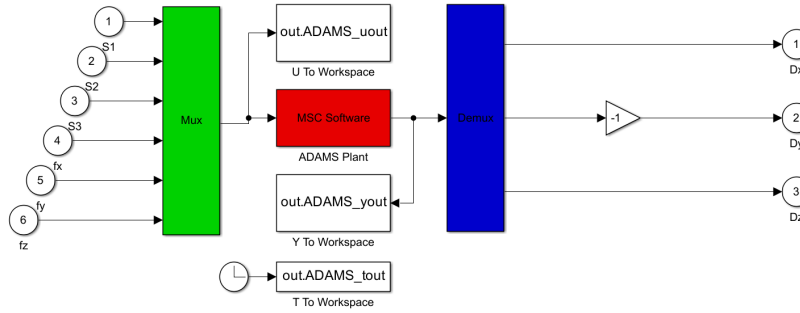

Fig. 8. Simplified ADAMS sub-block of co-simulation control system

4.2. Practical implementation of vibration detection

In the actual physical system, the *z*-direction vibration displacement of the thermal nozzle can be measured using high-precision non-contact laser displacement sensors or Micro-Electro-Mechanical Systems (MEMS) based accelerometers installed near the nozzle tip. The laser sensor offers micrometer-level accuracy and high response speed, making it suitable for capturing small-amplitude vibrations in real time. Alternatively, MEMS accelerometers can be used to detect acceleration signals, which are then integrated to obtain displacement information through a digital filter.

The measured signals are transmitted to the control system through a high-speed data acquisition module and processed in real time by the ES-FXLMS controller implemented in the Simulink environment. This configuration allows the same adaptive vibration suppression algorithm used in the simulation to be directly applied in practical HIL validation. The additional implementation details ensure that the proposed vibration detection and control strategy can be effectively transferred from simulation to an actual Delta-type additive manufacturing platform.

4.3. Integrated control system

Fig. 9 presents the Simulink block diagram of the integrated motion and vibration suppression control system based on the FXLMS algorithm. The system primarily consists of four modules: a trajectory input module, a PID control and inverse kinematics module, an FXLMS-based vibration control module, and a motor feedback module.

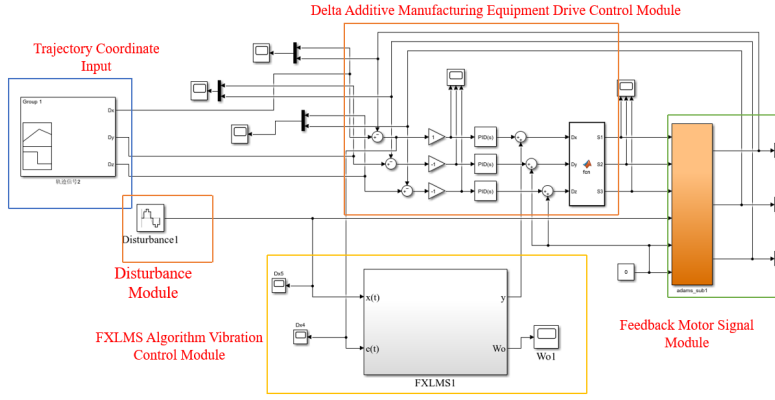

Fig. 9. Simulink simulation model of the integrated motion and vibration suppression control system

Specifically, the trajectory input module receives the desired path signal and serves as the system input. The PID control and inverse kinematics module adjusts trajectory errors and converts them into motor drive parameters. The FXLMS vibration control module adaptively

adjusts filter weights based on external disturbances and feedback signals, enabling active suppression of structural vibrations. The motor feedback module returns parameters such as displacement and current from the motion process back to the control system, enabling closed-loop correction and dynamic optimization.

By integrating motion control and vibration suppression into a unified control strategy, the system significantly enhances the operational accuracy and dynamic stability of the 3D printing device.

4.4. Simulation results and analysis

An integrated motion control model for the thermal nozzle system was developed based on a co-simulation platform combining MATLAB/Simulink and ADAMS. This model was designed to evaluate the response performance and tracking accuracy of a multi-axis control strategy across different motion directions. The overall simulation framework comprises a PID-based motion controller, an FXLMS adaptive filter module for active vibration suppression, a disturbance input module, and an ADAMS-based dynamic subsystem.

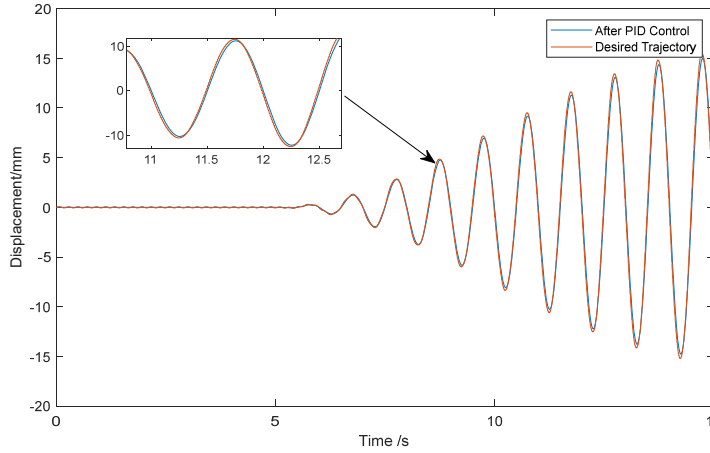

Fig. 10. Comparison of motion trajectories along the x-axis with and without PID control

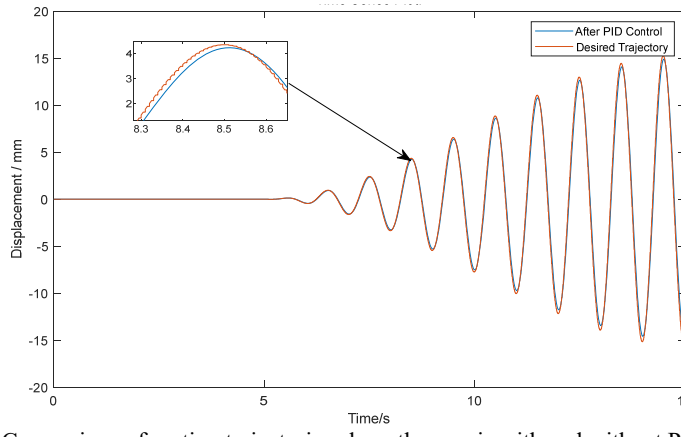

Fig. 11. Comparison of motion trajectories along the y-axis with and without PID control

The control architecture utilizes a triple closed-loop feedback configuration to independently manage trajectory tracking along the x, y, and z axis. The simulation duration was set to 5 seconds with a fixed time step of 0.0001 seconds. Controller parameters were iteratively tuned and

optimized based on system response characteristics. To emulate external disturbances, a step function was applied as the initial input excitation.

Simulation results were analyzed by extracting the response trajectories along the x, y, and z axis. These results were used to assess the system's tracking stability under the proposed integrated control scheme. The application of the PID controller enabled the system to maintain close alignment with the desired trajectory, with negligible steady-state error and smooth transient response. These findings demonstrate the effectiveness of the PID strategy in improving trajectory precision and maintaining overall system stability.

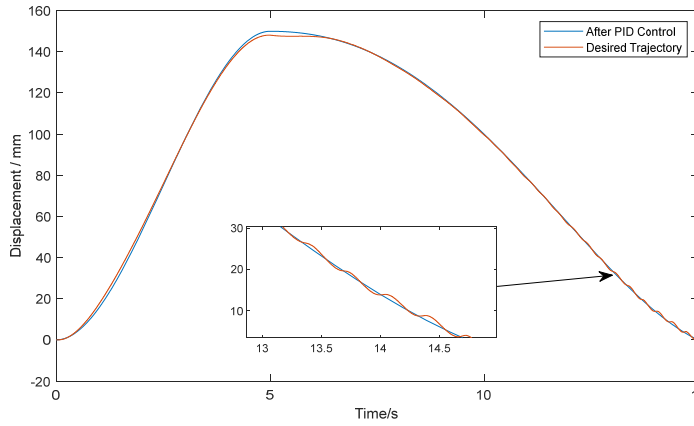

Fig. 12. Comparison of motion trajectories along the z-axis with and without PID control

The PID gains were tuned using a relay-based auto-tuning procedure in Simulink. Relay feedback was used to induce a stable limit cycle, from which the critical frequency characteristics were estimated for controller tuning. The tuning targeted a compromise between response speed and robustness. Frequency-domain verification of the tuned controller indicated a phase margin of approximately 65°, providing adequate stability margins against modeling uncertainties and external disturbances. After iterative validation, the final gains were selected as $K_p = 200$, $K_i = 10$, and $K_d = 9$. Further increases in the gains amplified oscillations and degraded stability, confirming the suitability of the chosen parameter set.

Motion control simulations were performed along all three axes of the Delta-type additive manufacturing system. Figs. 10-12 present a representative case in which the actual trajectory under classical PID control (blue) is compared with the desired trajectory (red). The results reveal that the system achieves PID convergence and high short-term tracking accuracy during the initial phase. A magnified view in the top-left corner highlights the reduced dynamic deviation at the trajectory peak.

In the subsequent vibration phase, although residual oscillations persist, the overall deviation from the desired trajectory is significantly reduced, confirming the PID controller's disturbance suppression capability and trajectory consistency. However, conventional PID control proves insufficient for maintaining long-term stability under periodic disturbances.

From a quantitative perspective, the deviation between the actual and desired trajectories under PID control remained within ±0.18 mm for most of the motion process, meeting the typical accuracy requirement of ±0.2 mm in high-precision additive manufacturing. The convergence time was approximately 0.45 seconds, indicating good responsiveness to short-term commands. Nevertheless, sustained disturbances continued to affect trajectory stability in later stages.

To address this, a reference trajectory modulation strategy was introduced to further enhance dynamic performance. This method maintained high tracking accuracy throughout the motion process and effectively suppressed the amplification of vibrations in the later stages. Simulations along the x, y, and z axis validated the effectiveness of the proposed strategy in improving both

motion quality and system robustness.

With this strategy applied, the peak deviation was further reduced to ±0.08 mm, significantly enhancing trajectory stability under dynamic loads. Compared to traditional PID control, the proposed method reduced the steady-state error by approximately 65 % and improved convergence speed by about 30 %. These findings demonstrate its adaptability and superior performance in practical additive manufacturing scenarios, particularly where vibration suppression is critical to ensuring part quality.

To further evaluate the effectiveness of the proposed active vibration control approach, a comparative analysis was conducted between the FXLMS based control strategy and conventional passive damping. Under identical disturbance conditions, the vibration responses of the thermal nozzle were recorded for both cases. We confirm that the active control strategy clearly outperformed passive damping in terms of suppression depth and convergence speed.

Moreover, passive damping devices are inherently limited by fixed parameters and structural constraints, making them less suitable for dynamic environments. In contrast, the proposed FXLMS-based control demonstrates real-time adaptability and effectively suppressed vibration energy within the 10-100 Hz range by over 40 dB in just 0.3 seconds, as verified by simulation data. This confirms its potential for application in space-constrained, dynamically varying environments such as orbital additive manufacturing platforms.

4.4.1. Single-frequency disturbance excitation

The vibration control algorithm was simulated in the printer's ADAMS environment, with the focus on vibration suppression along the x-axis. The choice to implement vibration control along the x-direction was based on the significant influence of disturbances and mechanical flexibilities in this particular direction. As the x-axis typically handles substantial dynamic loads and high-speed movements, it is more susceptible to vibration-induced deviations. Therefore, controlling vibration along the x-axis ensures more effective suppression of unwanted oscillations, leading to improved overall system stability and trajectory accuracy in the additive manufacturing process. Fig. 13 presents the vibration displacement curves of the thermal nozzle along a single degree of freedom under different control methods. When using passive damping, the nozzle exhibits relatively large vibrations and requires a longer time to stabilize. In contrast, the standard FXLMS algorithm significantly reduces vibration amplitude and ensures PID convergence. Furthermore, with the implementation of the ES-FXLMS algorithm proposed in this study, the suppression effect becomes more pronounced, achieving even better vibration mitigation performance.

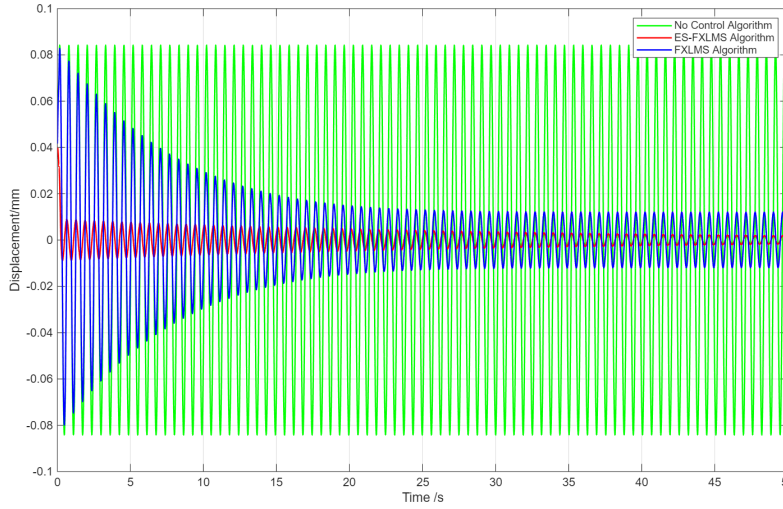

Fig. 13. Vibration suppression performance of three control strategies

Fig. 14 compares the power spectral density (PSD) of the thermal nozzle system under three control strategies: no control (green), FXLMS (blue), and the proposed ES-FXLMS algorithm (red). As shown, the ES-FXLMS algorithm achieves significantly deeper attenuation at dominant disturbance frequencies (e.g., 200 Hz, 300 Hz, 400 Hz). These harmonic peaks correspond to the system's structural modal frequencies, which are prone to resonant amplification under periodic excitation. Suppressing these frequencies is therefore critical for maintaining structural stability and ensuring print quality in Delta-type additive manufacturing systems.

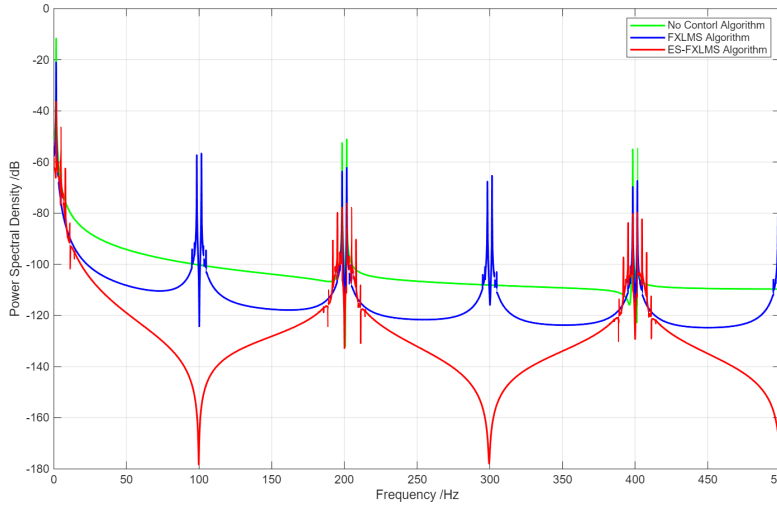

Fig. 14. Comparison of power spectral density (PSD) under noise disturbances

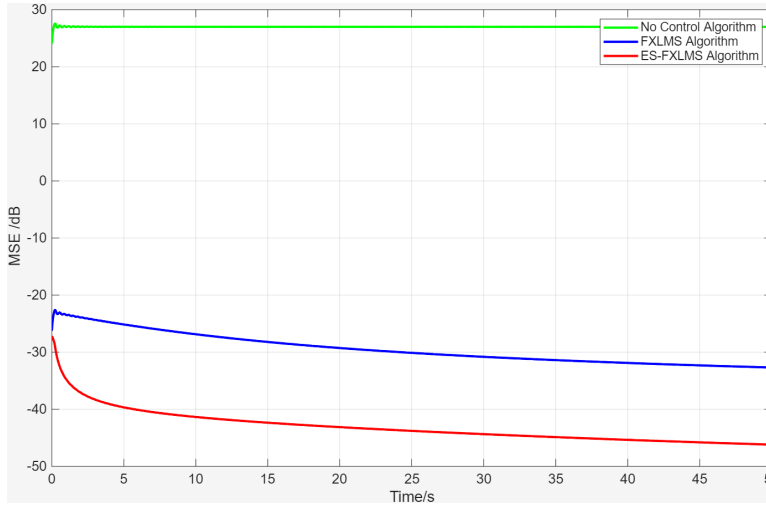

Fig. 15. MSE convergence curves of different algorithms under noise disturbances

The spectral peaks under the ES-FXLMS algorithm are markedly lower than those of the other two methods, indicating stronger attenuation across the target harmonic bands. The simulation was conducted over a 5-second duration with a sampling rate of 10 kHz and a time step of 0.0001 seconds. The external disturbance was modeled as a 10 Hz sinusoidal input with an amplitude of 1 mm.

These results validate the superior frequency-domain suppression capability of the proposed control strategy. While the FXLMS algorithm provides partial attenuation, it demonstrates limited suppression depth and narrower effective bandwidth. In contrast, the uncontrolled system exhibits

pronounced harmonic amplification, with vibrational energy distributed across multiple frequency bands. This comparison highlights the ES-FXLMS algorithm's effectiveness in addressing resonance-related issues and supports its engineering applicability in complex vibration scenarios.

In practical engineering environments, structural vibrations are often induced by complex and unpredictable external disturbances. To evaluate the robustness of the control algorithms under such conditions, broadband white noise was introduced in the simulation, superimposed with sinusoidal components corresponding to the system's modal frequencies. This approach emulates real-world excitation and allows comprehensive performance evaluation.

To assess both dynamic response and steady-state behavior, the total mean square error (TMSE) – defined as the cumulative MSE over the full simulation time – was adopted as the evaluation metric. Fig. 15 presents the time-domain evolution of MSE under noise interference for the three algorithms. For clarity, the MSE was smoothed, and TMSE values were used to quantify the overall control performance.

From the curve trends, it is evident that the ES-FXLMS algorithm (red line) consistently maintains the lowest MSE throughout the simulation, outperforming both the FXLMS (blue) and the uncontrolled system (green). The ES-FXLMS algorithm achieves a TMSE of 1.18, compared to 26.92 and 249.79 for the FXLMS and no-control cases, respectively. This reflects a 95.6 % reduction relative to FXLMS, and over 99.5 % reduction compared to the uncontrolled case.

In the context of trajectory control, a TMSE below 2.0 typically corresponds to a peak displacement error within ±0.1 mm, which aligns with the accuracy requirements of high-precision additive manufacturing. The proposed algorithm not only meets this tolerance but significantly exceeds it, demonstrating its feasibility for deployment in precision-critical applications.

Although the uncontrolled case may exhibit a gradual reduction in error due to passive dissipation, it shows much larger residual oscillations and substantially slower stabilization than the controlled cases. In contrast, the ES-FXLMS algorithm achieves faster convergence and maintains smoother and more stable error suppression throughout the process.

All three algorithms show relatively fast initial convergence. However, only the ES-FXLMS algorithm continues to reduce error consistently and maintain long-term stability, confirming its adaptability and robustness under time-varying and noisy disturbance conditions. These observations demonstrate the practical value of the proposed control strategy for enhancing the reliability and precision of Delta-type additive manufacturing systems in real-world environments.

To quantitatively evaluate the vibration suppression performance of each control algorithm, the Total Mean Square Error (TMSE) and Convergence Time are adopted as the primary performance indicators. TMSE represents the average energy of the residual vibration error throughout the control process, where a smaller value indicates higher steady-state accuracy and better suppression stability. Convergence time is defined as the time required for the algorithm to reach the steady state after a disturbance, indicating the system's dynamic response speed and adaptability. Therefore, an effective vibration suppression algorithm should achieve both a low TMSE and a short convergence time, ensuring rapid stabilization and minimal residual vibration. The combined comparison of these two metrics provides a comprehensive assessment of the algorithm's suppression efficiency and robustness under complex space disturbance conditions.

Table 3. Comparative performance of control strategies under disturbance conditions

Algorithm	Total mean square error (m^2)	Convergence time (s)
No vibration suppression	249.79	4.75
FXLMS algorithm	26.92	2.7
ES-FXLMS algorithm	1.18	1.85

To provide a deeper understanding of the early-stage convergence behavior of the ES-FXLMS algorithm, an additional quantitative analysis was performed based on the time-domain response curves obtained in simulation. As shown in Fig. 13, although the full steady-state convergence

requires approximately 1.85 s, the algorithm exhibits an extremely rapid initial reduction in residual vibration error. In particular, within the first 0.15-0.20 s, the error amplitude decreases by more than 70 %, effectively removing the dominant vibration components before entering the fine-tuning phase. This demonstrates that the ES-FXLMS algorithm achieves its essential suppression capability well ahead of full convergence.

This behavior is directly attributed to the nonlinear variable step-size mechanism, in which the exponentially decaying term provides a large initial adaptation gain, accelerating the suppression of strong vibration components, while the sinusoidal modulation further enhances responsiveness under slowly varying disturbances. The combination of these two mechanisms results in a convergence profile fundamentally different from the standard FXLMS family, where initial convergence is often much slower.

Furthermore, the early-stage suppression performance indicates that the algorithm's practical effective convergence time is substantially shorter than the theoretical time required to reach full steady-state. Since the disturbances in space-based FDM are continuous and gradually varying rather than abruptly changing, the adaptive filter rapidly aligns itself with the disturbance characteristics during the initial phase and spends the remaining convergence period only refining the residual micro-vibrations. Such a convergence pattern ensures that the algorithm can provide reliable vibration suppression even when the layer deposition time is as short as 0.2-0.5 s.

4.4.2. Dual-frequency disturbance excitation

In the dual-frequency disturbance experiment, the No Control Algorithm was replaced with the NLMS Algorithm to assess the performance improvement offered by an adaptive Algorithm like NLMS compared to an uncontrolled system. Unlike the No Control scenario, where the system remains susceptible to disturbances without any correction, the NLMS Algorithm actively adapts to the changing disturbance conditions, resulting in better disturbance rejection and faster convergence. This makes the system more robust and capable of effectively suppressing vibration, even in complex disturbance environments, thus enhancing overall performance and stability.

To further evaluate the robustness of the proposed algorithm under such conditions and to better replicate realistic space vibration environments, a dual-tone sinusoidal excitation of 10 Hz and 25 Hz was selected. These frequencies were chosen based on modal analysis results and previously reported in-orbit vibration spectra, ensuring that both the primary structural resonance and representative higher-order disturbance components were covered. The vibration suppression performance of the three control algorithms was then systematically compared and analyzed under these excitation conditions.

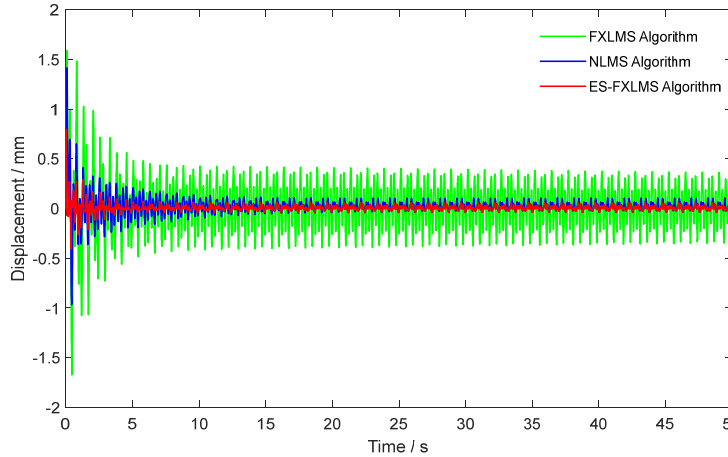

Fig. 16. Vibration suppression performance of three control strategies

ISSN PRINT 1392-8716, ISSN ONLINE 2538-8460

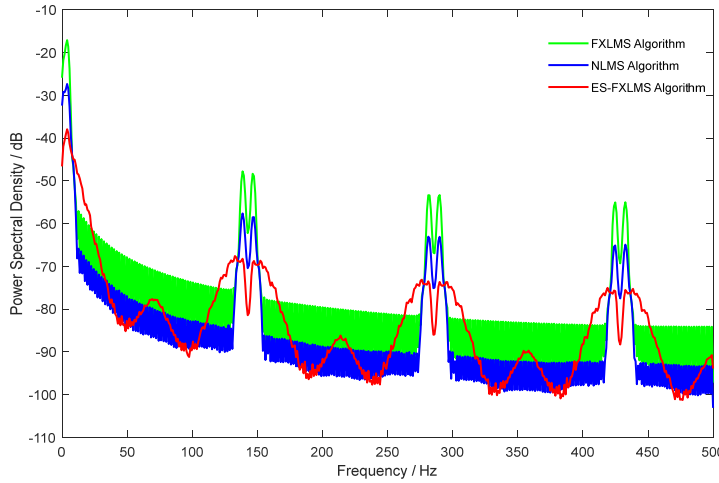

Fig. 17. Comparison of power spectral density (PSD) under noise disturbances

To provide a more scientific and comprehensive evaluation of the proposed ES-FXLMS algorithm, the NLMS algorithm was deliberately selected for comparison instead of the uncontrolled case. The rationale behind this choice is that NLMS employs a normalized step-size adjustment based on the instantaneous power of the reference signal, representing a classical and practically robust variant of the LMS family widely adopted in engineering applications. By comparing FXLMS, NLMS, and ES-FXLMS, the proposed method can be evaluated in terms of convergence rate, steady-state accuracy, and robustness under complex space disturbance conditions, thereby demonstrating its suitability for active vibration control under complex space disturbance environments.

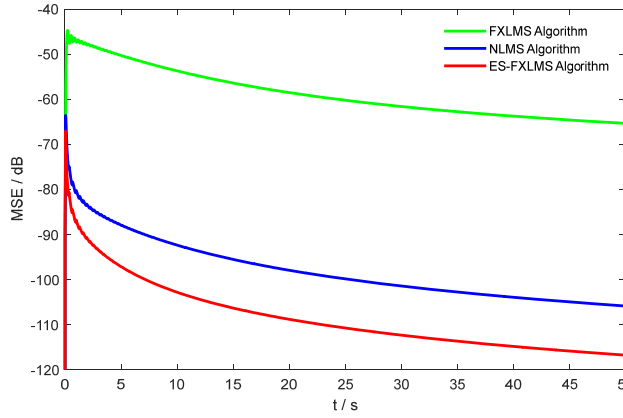

Fig. 18. MSE convergence curves of different algorithms under noise disturbances

Simulation results indicate that under dual-frequency excitation, the vibration suppression performance of all three algorithms declines compared to the single-tone or white-noise excitation cases. Specifically, under single-frequency excitation, the residual vibration amplitude can be suppressed below 0.02 mm, whereas under dual-frequency excitation, it remains below 0.05 mm. Regardless of the disturbance type, the ES-FXLMS algorithm consistently achieves the most significant reduction in vibration amplitude. Under dual-frequency excitation, the peak amplitudes of the FXLMS and NLMS algorithms are nearly identical, whereas ES-FXLMS maintains superior suppression.

A quantitative comparison of convergence time and steady-state error is summarized in

Table 3. Even under complex dual-frequency disturbances, ES-FXLMS achieves faster convergence and higher steady-state accuracy than the other two algorithms, confirming its strong adaptability and robustness for active structural vibration control.

Table 4. Comparative performance of control strategies under disturbance conditions

Algorithm	Total mean square error (m^2)	Convergence time (s)
FXLMS algorithm	4742.35	47.2
NLMS algorithm	549.3	23.8
ES-FXLMS algorithm	69.71	10.9

5. Conclusions

This study developed an integrated motion-vibration control strategy for Delta-type space-based FDM systems, which explicitly addresses the coupling between trajectory tracking and adaptive vibration suppression under space micro-disturbance environments. The proposed framework combines PID trajectory control with an enhanced ES-FXLMS adaptive vibration suppression algorithm. A high-fidelity ADAMS-Simulink co-simulation platform was established to evaluate the control performance under representative space micro-vibration conditions.

Under single-frequency disturbances, the proposed ES-FXLMS algorithm reduced the residual vibration amplitude to below 0.02 mm, achieving an improvement of over 80 % compared with FXLMS and over 70 % compared with NLMS. In the more challenging dual-frequency disturbance scenario, ES-FXLMS maintained a residual vibration amplitude of below 0.05 mm, yielding a TMSE reduction of approximately 87 % relative to FXLMS and 78 % relative to NLMS. Moreover, ES-FXLMS demonstrated the fastest transient decay, with more than 60 % error reduction within the first 0.2 s, enabling effective control even when the per-layer printing duration is as short as 0.2-0.5 s. Across all evaluated conditions, the integrated PID+ES-FXLMS framework consistently exhibited superior vibration attenuation, improved trajectory tracking accuracy, and enhanced system stability. These results confirm that the proposed method effectively addresses the multi-frequency, broadband, and time-varying disturbances characteristic of space-based additive manufacturing. This performance gain is primarily attributed to the proposed nonlinear variable step-size mechanism, which effectively balances fast convergence and steady-state robustness under time-varying disturbances.

Nevertheless, several limitations remain in the present study. The proposed method has so far been validated only within a high-fidelity simulation environment, and its real-world performance has yet to be confirmed through hardware experimentation. In addition, the dynamic model adopted in this work is based on small-amplitude linearization, which neglects nonlinear effects such as large-motion coupling, Coriolis forces, and centrifugal forces – factors that may become significant under high-speed or large-range operational conditions. Furthermore, the current control strategy relies on independent-axis regulation, which, while sufficient for the moderately coupled scenarios considered here, may not adequately address stronger dynamic coupling that can arise in more complex working conditions.

To address these issues, future work will focus on conducting HIL experiments using a space-based additive manufacturing prototype to further validate the algorithm's real-time performance and robustness. Efforts will also be directed toward extending the dynamic model to incorporate nonlinear and time-varying behaviors, and toward developing multi-Axis coordinated control strategies capable of more effectively handling strong coupling effects. Ultimately, the proposed control framework will be further refined and integrated into real on-orbit fabrication systems to support practical space manufacturing applications.

In summary, the integrated control method proposed in this study demonstrates strong robustness, adaptability, and effectiveness in mitigating high-frequency micro-vibrations in space-based FDM processes. The findings provide a solid technical foundation for enhancing the accuracy, stability, and real-time controllability of future space additive manufacturing missions.

Acknowledgements

This work was supported by Jiangsu Provincial Natural Science Foundation (SBK2024046179).

Data availability

The datasets generated during and/or analyzed during the current study are available from the corresponding author on reasonable request.

Author contributions

Yuchen Yang: Conceptualization; methodology, formal analysis, investigation, data curation, visualization, writing-original draft preparation, writing-review and editing. Yubin Fang: supervision, project administration, resources, funding acquisition.

Conflict of interest

The authors declare that they have no conflict of interest.

References

[1] D. Li et al., "Additive manufacturing – a revolutionary technology for aerospace manufacturing," (in Chinese), *Acta Aeronautica et Astronautica Sinica*, Vol. 43, No. 4, 2022, https://doi.org/10.7527/s1000-6893.2021.25387

[2] J. Zhang, G. Wang, X. Chen, and X. Li, "Applications of 3D printing in large-scale space construction," (in Chinese), *Space Electronic Technology*, Vol. 21, No. 5, pp. 11–17, 2024.

[3] H. Tang, Q. Sun, Z. Li, X. Su, and W. Yan, "Longitudinal compression failure of 3D printed continuous carbon fiber reinforced composites: An experimental and computational study," *Composites Part A: Applied Science and Manufacturing*, Vol. 146, p. 106416, Jul. 2021, https://doi.org/10.1016/j.compositesa.2021.106416

[4] Z. You, W. Zhang, J. Shen, Y. Ye, X. Ye, and S. Zhou, "Adaptive neural network vibration suppression control of flexible joints space manipulator based on H∞ theory," *Journal of Vibroengineering*, Vol. 25, No. 3, pp. 492–505, May 2023, https://doi.org/10.21595/jve.2022.22797

[5] M. H. Korayem, M. Bamdad, H. Tourajizadeh, A. H. Korayem, and S. Bayat, "Analytical design of optimal trajectory with dynamic load-carrying capacity for cable-suspended manipulator," *The International Journal of Advanced Manufacturing Technology*, Vol. 60, No. 1-4, pp. 317–327, Aug. 2011, https://doi.org/10.1007/s00170-011-3579-9

[6] S. Khan, K. Joshi, and S. Deshmukh, "A comprehensive review on effect of printing parameters on mechanical properties of FDM printed parts," *Materials Today: Proceedings*, Vol. 50, pp. 2119–2127, Jan. 2022, https://doi.org/10.1016/j.matpr.2021.09.433

[7] K. Yu, Z. Zhang, Z. Zhou, and M. Dai, "A modified Bresenham algorithm for control system of FDM three-dimensional printer," *Mechatronics and Machine Vision in Practice 4*, pp. 125–139, Sep. 2020, https://doi.org/10.1007/978-3-030-43703-9_11

[8] O. V. Zakharov, K. G. Pugin, and T. N. Ivanova, "Modeling and analysis of delta kinematics FDM printer," in *Journal of Physics: Conference Series*, Vol. 2182, No. 1, p. 012069, Mar. 2022, https://doi.org/10.1088/1742-6596/2182/1/012069

[9] P. Wu, C. Qian, and C. E. Okwudire, "Design, modeling and feedforward control of a hybrid extruder for material extrusion additive manufacturing," *Additive Manufacturing*, Vol. 92, p. 104378, Jul. 2024, https://doi.org/10.1016/j.addma.2024.104378

[10] N. Edoimioya, C.-H. Chou, and C. E. Okwudire, "Vibration compensation of delta 3D printer with position-varying dynamics using filtered B-splines," *The International Journal of Advanced Manufacturing Technology*, Vol. 125, No. 5-6, pp. 2851–2868, Jan. 2023, https://doi.org/10.1007/s00170-022-10789-w

[11] J. Wang, J. Liao, L. He, X. Tan, and Z. Chen, "Variable step-size FxLMS algorithm based on cooperative coupling of double nonlinear functions," *Symmetry*, Vol. 17, No. 8, p. 1222, Aug. 2025, https://doi.org/10.3390/sym17081222

[12] X. Sun, Y. Qu, F. Wang, and J. Xu, "Effects of time-delayed vibration absorber on bandwidth of beam for low broadband vibration suppression," *Applied Mathematics and Mechanics*, Vol. 44, No. 10, pp. 1629–1650, Sep. 2023, https://doi.org/10.1007/s10483-023-3038-6

[13] A. Ali, M. Moinuddin, and T. Y. Al-Naffouri, "NLMS is more robust to input-correlation than LMS: a proof," *IEEE Signal Processing Letters*, Vol. 29, pp. 279–283, Jan. 2022, https://doi.org/10.1109/lsp.2021.3134141

[14] D. Bismor, K. Czyz, and Z. Ogonowski, "Review and comparison of variable step-size LMS algorithms," *The International Journal of Acoustics and Vibration*, Vol. 21, No. 1, pp. 24–39, Jan. 2016, https://doi.org/10.20855/ijav.2016.21.1392

[15] Y. Zhang, W. Yang, D. Wei, D. Zhang, and X. Yang, "Energy dissipation of tuned magnetic fluid rolling-ball damper in low-frequency vibration," *IEEE Transactions on Magnetics*, Vol. 59, No. 4, pp. 1–11, Apr. 2023, https://doi.org/10.1109/tmag.2023.3248864

[16] C. Liang, Q. Shen, and K. Wang, "Active vibration suppression method for the thermal nozzle of space FDM equipment," (in Chinese), *Intelligent Internet of Things Technology*, Vol. 57, No. 5, pp. 123–131, 2025, https://doi.org/10.26921/j.cnki.2096-6059.2025.05.025

[17] Y. Xu, Z. Ye, and S. Wu, "Pose tracking control of rigid-flexible coupled space robots based on singular perturbation theory," (in Chinese), *Science China: Physics, Mechanics and Astronomy*, 2025.

[18] W. Li, Z. Yang, K. Li, and W. Wang, "Hybrid feedback PID-FxLMS algorithm for active vibration control of cantilever beam with piezoelectric stack actuator," *Journal of Sound and Vibration*, Vol. 509, p. 116243, Sep. 2021, https://doi.org/10.1016/j.jsv.2021.116243

[19] G. Modi and B. Singh, "A novel multilayer N-LMS adaptive-filter-based control for synchronization and power quality improvement in Grid-Tied SPV system," *IEEE Transactions on Industrial Electronics*, Vol. 70, No. 9, pp. 9158–9168, Sep. 2023, https://doi.org/10.1109/tie.2022.3215826

[20] N. Madani and E. J. M. Carranza, "Co-simulated size number: an elegant novel algorithm for identification of multivariate geochemical anomalies," *Natural Resources Research*, Vol. 29, No. 1, pp. 13–40, Aug. 2019, https://doi.org/10.1007/s11053-019-09547-9

[21] F. Cappuzzo, D. Bianchi, V. Dezobry, and S. Digennaro, "A novel co-simulation framework for verification and validation of GNC algorithms for autonomous UAV," in *Vertical Flight Society 78th Annual Forum and Technology Display*, May 2022.

[22] X. Liu, H. Wu, and W. Xiao, "Improved variable step-size adaptive algorithm based on a dual-sigmoid function and its application in OCT," (in Chinese), *Journal of Electronics*, Vol. 47, No. 1, pp. 234–240, 2019.

[23] X. Li, "Research progress on process control issues of 3D printing technology," (in Chinese), *Acta Automatica Sinica*, Vol. 42, No. 7, pp. 983–1003, 2016, https://doi.org/10.16383/j.aas.2016.c150619

[24] A. Xu, "Research on integrated pointing and vibration isolation technology for ultra-large space telescopes," (in Chinese), University of Chinese Academy of Sciences, 2025, https://doi.org/10.27522/d.cnki.gkcgs.2025.000030

[25] B. Li et al., "Research on variable-step-size adaptive filter algorithm with a momentum term," *Applied Sciences*, Vol. 13, No. 21, p. 12077, Nov. 2023, https://doi.org/10.3390/app132112077

[26] R. Zheng et al., "VssL-MMSE: a variable step-size optimization algorithm for high-speed SerDes adaptive equalizer," *Journal of Circuits, Systems and Computers*, Vol. 35, No. 7, Nov. 2025, https://doi.org/10.1142/s0218126625504870

[27] F. Wang and J. Du, "A variable step-size LMS adaptive filtering algorithm based on error feedback," in *International Conference on Education Technology and Information System*, 2013.

Yuchen Yang is a graduate student in Mechanical Engineering at Jiangsu University of Technology, Changzhou, China. His research interests include active vibration control, mechanical dynamics, and advanced manufacturing.

Yubin Fang received the Ph.D. degree in 2020. He is currently a lecturer and M.S. supervisor at Jiangsu University of Technology, Changzhou, China. His research interests include active vibration control and adaptive control methods. He has published several research papers, including "A novel variable step size least mean square method for adaptive micro-vibration control" in the Journal of Vibration and Control (2022, Vol. 28, Nos. 19-20).